Improper magnetic ferroelectricity of nearly pure electronic nature in helicoidal spiral $CaMn_7O_{12}$

Jin Soo Lim, Diomedes Saldana-Greco, and Andrew M. Rappe
Department of Chemistry, University of Pennsylvania, Philadelphia, Pennsylvania 19104-6323, USA

(Received 12 January 2016; published 11 January 2018)

Helicoidal magnetic order breaks inversion symmetry in quadruple perovskite $CaMn_7O_{12}$, generating one of the largest spin-induced ferroelectric polarizations measured to date. Here, the microscopic origin of the polarization, including exchange interactions, coupling to the spin helicity, and charge density redistribution, is explored via first-principles calculations. The *B*-site Mn^{4+} (Mn3) spin adopts a noncentrosymmetric configuration, stabilized not only by spin-orbit coupling (SOC), but also by the fully anisotropic Hubbard *J* parameter in the absence of SOC, to break inversion symmetry and generate polarization. Berry phase computed polarization ($P_{\mathrm{elec}} = 2169\,\mu\mathrm{C/m^2}$) exhibits nearly pure electronic behavior, with negligible Mn displacements ($\approx$0.7 mÅ). Orbital-resolved density of states shows that *p-d* orbital mixing is microscopically driven by nonrelativistic exchange striction within the commensurate ionic structure. Persistent electronic polarization induced by helical spin order in the nearly inversion-symmetric ionic crystal lattice suggests opportunities for ultrafast magnetoelectric response.

DOI: 10.1103/PhysRevB.97.045115

I. INTRODUCTION

Multiferroics, simultaneously displaying ferroelectricity and intrinsic magnetic ordering, have gained much attention due to the complex physics underlying the magnetoelectric effect and its potential applications in spin-driven electronics [1,2]. Based on the nature of the order-parameter coupling, multiferroics are classified into type I and type II [3]. Type I consists of $6s^2$ lone-pair proper ferroelectrics [4–6] and improper ferroelectrics of electronic [7] and geometric origins [8] including hybrid improper ferroelectrics [9], where ferroelectricity remains largely independent of magnetism. Type II essentially refers to improper magnetic ferroelectrics, where spin ordering breaks inversion symmetry, resulting in ionic displacements and/or electronic charge redistribution that provide macroscopic polarization. Numerous examples include (a) cycloidal spiral systems [10–17], (b) triangular lattice systems with proper screw-type spiral [18–22], and (c) exchange striction systems with collinear magnetism [23–26]. Despite relatively small polarization and low Curie temperature, type-II multiferroics can potentially lead to the design of robust room-temperature multiferroics with large spontaneous polarization and ultrafast switchability.

Historically, three microscopic models have been established in the literature [27–30]. First, the exchange striction model proposes that nonrelativistic symmetric exchange interactions in a $\uparrow\uparrow\downarrow\downarrow$ spin order cause electronic charge density to shift and/or ferromagnetically coupled ions to move toward each other, generating $\boldsymbol{P}_{12} \propto \boldsymbol{e}_{12}\,(\boldsymbol{S}_1 \cdot \boldsymbol{S}_2)$. Here, $\boldsymbol{P}_{12}$ is the intersite vector polarization, and $\boldsymbol{e}_{12}$ is a unit vector connecting the two magnetic ions. Second, the spin-current (KNB) model [31], also known as KNB (Katsura-Nagaosa-Balatsky) model and analytically equivalent to the inverse Dzyaloshinskii-Moriya (DM) model [24], is derived from spin-orbit coupling (SOC). Here, electronic charge density and/or nonmagnetic anions shifts in response to relativistic DM interaction between the two canted spin sites, generating $\boldsymbol{P}_{12} \propto \boldsymbol{e}_{12} \times (\boldsymbol{S}_1 \times \boldsymbol{S}_2)$. Third, in the spin-dependent *p-d* hybridization model, SOC causes an intrasite polarization along the metal-ligand bond, $\boldsymbol{P}_{\mathrm{ml}} \propto (\boldsymbol{S}_{\mathrm{m}} \cdot \boldsymbol{e}_{\mathrm{ml}})^2\,\boldsymbol{e}_{\mathrm{ml}}$ [20,32,33], where $\boldsymbol{e}_{\mathrm{ml}}$ is the metal-ligand unit vector. While these three models are microscopic in nature, they depend on specific crystal lattice geometries.

Recently, a phenomenological model for spin-induced ferroelectricity has been shown to be capable of reproducing the aforementioned microscopic models as its limiting subcases [34]. The model first distinguishes between the ionic and the electronic contributions to the total polarization. Spin-induced ionic displacements have been reported to be small, usually less than 10 mÅ. Electronic contribution consists of intrasite (single-site) and intersite polarization. The intrasite term corresponds to the spin-dependent *p-d* hybridization term and is considered negligible in most cases. The intersite term consists of the exchange striction term $[\propto (\boldsymbol{S}_1 \cdot \boldsymbol{S}_2)]$ and the spin-current term $[\propto (\boldsymbol{S}_1 \times \boldsymbol{S}_2)]$, the latter of which was originally formulated in the generalized spin-current model [35]. Here, $\boldsymbol{S}_1$ and $\boldsymbol{S}_2$ are the vector spins on the two neighboring sites 1 and 2. It is important to note that this model is phenomenological and does not by itself provide any microscopic information unless accompanied by first-principles analysis.

$CaMn_7O_{12}$ manifests one of the largest spin-induced polarizations measured to date ($P = 2870\,\mu\mathrm{C/m^2}$) [36]. Exchange striction has been proposed as the main microscopic mechanism [37–39], with small SOC contribution from the spin-dependent *p-d* hybridization [38], as well as inverse-DM contribution in the presence of structural modulation [39,40]. However, the exact role of ionic displacements and the origin of the polarization direction require further clarification and analysis.

Here, we report on the ferroelectric polarization of nearly pure electronic nature in $CaMn_7O_{12}$ induced by its helicoidal magnetic ground state, computed via density functional theory (DFT) calculations. For simplicity and clarity, we preserve inversion symmetry on the ionic lattice while the charge density distribution is permitted to respond to the symmetry-breaking spin pattern; these changes to orbital mixing make the dominant contribution to the polarization. We employ

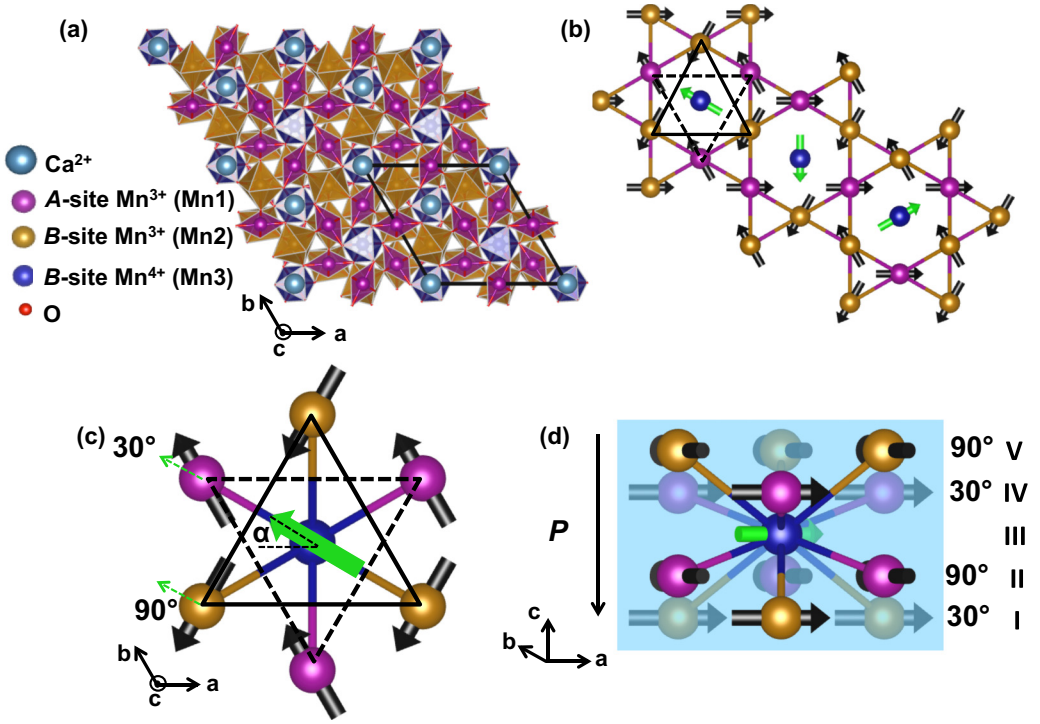

FIG. 1. (a) The crystal structure of the rhombohedral ($R\bar{3}$) phase. Mn1 (purple, square planar) and Mn2 (gold, octahedral) alternate along parallel c chains, of which sets of three form a Kagome lattice. The hexagonal center is occupied by Ca^{2+} (light blue) and Mn3 (blue, octahedral) alternating along the c axis. The unit cell is denoted with bold black lines. (b) Noncollinear magnetic structure with Mn1 and Mn2 spins represented as black arrows and Mn3 spins represented as green arrows. Black lines indicate the local hexagonal environment of Mn3 surrounded by Mn1 and Mn2, with solid lines closer to the viewer than dashed lines. (c) Zoom-in view of the local hexagonal environment in (b). Mn3 spin configuration is represented by α, where $\alpha = 30^\circ$ for (30°, 90°) configuration with respect to the neighboring (Mn1, Mn2) spins. (d) Side view of (c) showing the local layered structure of five Mn planes (I–V), magnetically inducing net polarization along the c axis. The blue plane is parallel to the c axis and cuts through the central Mn3, such that the atoms farther away from the viewer are shaded by the plane.

the Heisenberg-DM spin Hamiltonian to provide microscopic understanding of our first-principles observations.

The quadruple perovskite belongs to the $[AA'_3][B_4][O_{12}]$ family [41]: $[CaMn_3][Mn_4][O_{12}]$. $CaMn_7O_{12}$ undergoes structural and metal-insulator transition accompanied by charge ordering at $T = 440$ K with a large change in resistivity at ultrafast time scales [42,43]. The B-site Mn ions order into Mn^{3+} and Mn^{4+} with a 3 : 1 ratio in a centrosymmetric rhombohedral ($R\bar{3}$) crystal structure [Fig. 1(a)], such that the formula is rewritten as $[CaMn_3^{3+}][Mn_3^{3+}Mn^{4+}][O_{12}]$. Throughout this paper, A-site Mn^{3+} is designated as Mn1, B-site Mn^{3+} is designated as Mn2, and B-site Mn^{4+} is designated as Mn3.

$CaMn_7O_{12}$ exhibits complex coupling of incommensurate structural, orbital, and magnetic modulations. At $T = 250$ K, Jahn-Teller distortions lead to structural modulation mediated by orbital ordering, with structural propagation vector (0, 0, 2.077) at 150 K [39,40]. The material exhibits two magnetic phase transitions at Néel temperatures, $T_{N1} = 90$ K and $T_{N2} = 48$ K [36]. Between 90 and 48 K, Mn3 spin modulation is coupled to the structural modulation via a magneto-orbital helix, where the chiral magnetic structure with propagation vector (0, 0, 1.037) is stabilized by the orbital modulation [39,40,44]. Below 48 K, magnetic modulation with two propagation vectors (0, 0, 0.958) and (0, 0, 1.120) has been proposed [36].

All spins lie in the ab plane, and Mn ions along the same c chain or of the same Mn type and c-axis height have identical spin directions. Noncollinear magnetism arises nonrelativistically via geometric frustration of the spins within the hexagonal Kagome lattice [45–47], where antiferromagnetic interactions among Mn1 and Mn2 [37,40] cause all spin pairs in adjacent c chains to be 120° from each other [Fig. 1(b)]. The Mn3 spin direction is determined by the neighboring three Mn1s and three Mn2s. It has been proposed that Mn3 adopts a spin direction that is (30°, 90°) [36,37,48,49] or (60°, 60°) [38,50] with respect to the surrounding (Mn1, Mn2) spin directions. The Mn3 spin configuration is conveniently represented by the quantity α, where $\alpha = 0^\circ$ for (60°, 60°) and 30° for (30°, 90°) [Fig. 1(c)]. The sign of α corresponds to the spin helicity of the B-site helicoidal spin spiral. The local structure of the hexagonal channel consists of five equidistant ab planes (I–V) repeating periodically along the c axis, where the central layer consists of a single Mn3 [Fig. 1(d)]. The ferroelectric transition temperature of the material coincides with the Néel temperature, $T_C = T_{N1} = 90$ K, suggesting that the ferroelectricity is spin driven [36,51]. The macroscopic polarization is along the c axis ([111] in the pseudocubic coordinates), parallel to the spin helicity vector and perpendicular to the spin rotation plane (ab plane).

TABLE I. Berry phase computed P and converged Mn3 spin direction α with DFT+U+J with and without SOC.

	α	P (μC/m^2)
NSOC	−0.02°	−1.1
NSOC	29.0°	−2119
SOC	28.3°	−2169

II. METHOD AND COMPUTATIONAL DETAILS

We evaluate the noncollinear magnetic ground state using the PBEsol [52] functional with Hubbard U and J (on-site Coulomb repulsion and exchange parameters) treated separately and explicitly defined within the rotationally invariant, fully anisotropic scheme [53,54], along with SOC as implemented in the QUANTUM ESPRESSO [55] package. It has been demonstrated that the fully anisotropic Hubbard J parameter plays a central role in correctly describing spin canting in noncollinear magnetic systems [56]. All atoms are represented by norm-conserving, optimized [57], designed nonlocal [58] pseudopotentials generated with the OPIUM package [59], including spin-orbit interaction [60] as well as nonlinear core-valence interaction in the Mn pseudopotential via the partial-core correction scheme [61–63]. The plane-wave cutoff energy is set at 70 Ry (952 eV), and the total energy is converged to 10^{-6} Ry (1.4×10^{-5} eV) per 60-atom unit cell (3 formula units). The Brillouin zone is sampled using a $2 \times 2 \times 4$ Monkhorst-Pack [64] k-point mesh.

III. RESULTS AND DISCUSSION

The energetics and spin direction of collinear and noncollinear magnetic configurations are used to justify the values $U = 2$ eV and $J = 1.4$ eV used in our DFT calculations [65]. These values are in line with those used in previous studies [37–39,48,49]. We use the commensurate, centrosymmetric ionic lattice structure [66]. Starting from multiple perturbations of the commensurate noncollinear magnetic structure [36], our spin and electronic relaxation shows that the Mn1 and Mn2 spin directions remain ≈120° apart. The converged Mn3 spin direction depends strongly on Hubbard J and SOC. With $J < 1$ eV, α remains ≈0° without SOC, with deviations away from 0° upon applying SOC. Surprisingly, the experimentally observed $\alpha \approx 30°$ is achieved at $J = 1.4$ eV, both with and without SOC. If Mn3 spins are started at $\alpha = 0°$, they remain in that symmetry, showing that $\alpha = 0°$ is higher in energy by 0.54 meV per formula unit in the absence of SOC.

We use the Berry phase method [67] to compute the polarization P with and without SOC at different α values [68]. The most relevant scenarios with $\alpha \approx 0$ and 30° are shown in Table I. The polarization is along the c axis. Simultaneous ionic relaxation [69] gives Mn3 displacement of 0.7 mÅ with total $P = 2900\ \mu\text{C/m}^2$, in good agreement with the experimental value of $2870\ \mu\text{C/m}^2$ [36]. The ionic displacement is negligible relative to the thermal motion at $T_C = 90$ K, and it contributes 30% of the total polarization. At $\alpha \approx 0°$, the polarization vanishes; upon inverting the spin helicity by changing the sign of α, the direction of the polarization reverses with the same magnitude, in agreement with the phenomenological ferroaxial coupling proposed by Johnson *et al.* [36], as well as the sinusoidal dependence on α derived with the exchange striction model by Lu *et al.* [37].

Previous study by Cao *et al.* [39] reported contributions from nonrelativistic (exchange striction) as well as relativistic (inverse-DM) effects to the polarization upon employing local approximation of the incommensurate structural modulation. However, our results within the commensurate ionic structure indicate negligible contribution of SOC to the polarization (< 5%), suggesting that the bulk value arises from nonrelativistic effects. This observation is in alignment with Lu *et al.* [37], who proposed exchange striction as the main underlying mechanism.

The nonzero polarization at $\alpha \approx 30°$ indicates that inversion symmetry is broken, even though the ionic lattice is fixed to be centrosymmetric. Upon inversion operation along the B-site helicoidal spiral chains in each of the Cartesian directions ([100], [010], and [001]), only the $\alpha = 0°$ configuration is shown to preserve inversion symmetry [70].

We compute the charge density redistribution as the magnetic structure goes from $\alpha = 0$ to 30°, i.e., $\Delta\rho(\mathbf{r}) = \rho(\mathbf{r})_{\alpha=30°} - \rho(\mathbf{r})_{\alpha=0°}$ [Fig. 2]. The charge density isosurfaces reveal that the polarization is localized along the Mn3-O bonds. As discussed above, Mn3 ions do respond to the charge density redistribution but only by 0.7 mÅ, providing a minor contribution to the polarization. This indicates that the spin-induced ferroelectricity is nearly purely electronic in nature. Significant purely electronic contributions have also been predicted in orthomanganites [71–74].

To understand the relationship between α and P, we first rationalize the stabilization of $\alpha = 30°$ by Hubbard J in the absence of SOC. In contrast to DFT+U_{eff}, where J is subsumed under $U_{\text{eff}} = U - J$ [75], Hubbard U and J are defined distinctly in DFT+U+J [75], where the J parameter acts directly on the nondiagonal elements of the density matrix within the spinor representation that determine spin canting [56]. This treatment

TABLE II. Exchange energies for Mn3-V and Mn3-I interactions [76] for $\alpha = 0$ and 30°, with the total energy given by Eq. (4).

		E_{tot}	E_{SE}	E_{DM}
$\alpha = 0°$	Mn3-V	$3J\left(1 + \frac{1}{2}\gamma J_{\text{Hub}}\right)$	$\frac{3}{2}J\left(1 + \frac{1}{2}\gamma J_{\text{Hub}}\right)$	$-\frac{3\sqrt{3}}{2}D^z$
	Mn3-I		$\frac{3}{2}J\left(1 + \frac{1}{2}\gamma J_{\text{Hub}}\right)$	$\frac{3\sqrt{3}}{2}D^z$
$\alpha = 30°$	Mn3-V	$\frac{3}{2}\left[\sqrt{3}J\left(1 + \frac{\sqrt{3}}{2}\gamma J_{\text{Hub}}\right) - D^z\right]$	0	$-3D^z$
	Mn3-I		$\frac{3\sqrt{3}}{2}J\left(1 + \frac{\sqrt{3}}{2}\gamma J_{\text{Hub}}\right)$	$\frac{3}{2}D^z$

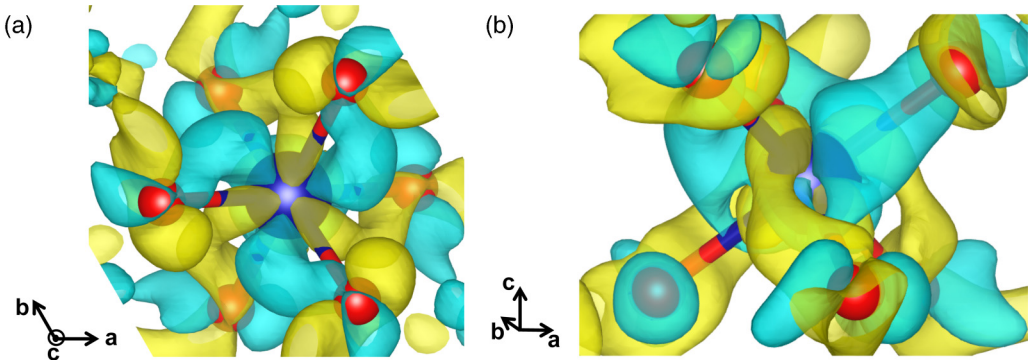

FIG. 2. Charge density redistribution along the Mn3-O bonds as the magnetic structure changes from $\alpha = 0$ to 30°. The charge density shift is purely electronic and nonionic. (a) Top and (b) side view of the charge density differential. The three Mn3-O bonds with $+c$ components gain electron density (cyan), whereas the three Mn3-O bonds with $-c$ components lose electron density (yellow), thereby generating a net polarization along the $-c$ direction.

results in an extra Hubbard energy correction term involving J that discourages interactions between electrons of antialigned spins on the same site, thereby encouraging magnetic ordering [54]:

$$E_{\mathrm{Hub}} = \sum_{I,\sigma} \frac{U^I - J^I}{2} \mathrm{Tr}[\boldsymbol{n}^{I\sigma}(\mathbf{1} - \boldsymbol{n}^{I\sigma})] + \sum_{I,\sigma} \frac{J^I}{2} (\mathrm{Tr}[\boldsymbol{n}^{I\sigma}\boldsymbol{n}^{I-\sigma}] - 2\delta_{\sigma\sigma_{\mathrm{min}}} \mathrm{Tr}[\boldsymbol{n}^{I\sigma}]). \quad (1)$$

Here, I is the atomic site index, σ is the spin index, σ_{min} denotes the minority spin, and $\boldsymbol{n}$ is the density matrix. By taking into account Hund's coupling, i.e., intra-orbital exchange, Hubbard J provides anisotropy and full orbital dependence across the occupations and energies of the Mn d states [77–79]. We believe that this anisotropy stabilizes $\alpha = 30°$ by modifying the nonrelativistic exchange interaction within the Heisenberg-DM spin Hamiltonian:

$$H_{12} = H_{\mathrm{SE}} + H_{\mathrm{DM}} = J_{12}(\boldsymbol{S}_1 \cdot \boldsymbol{S}_2) + \boldsymbol{D}_{12} \cdot (\boldsymbol{S}_1 \times \boldsymbol{S}_2). \quad (2)$$

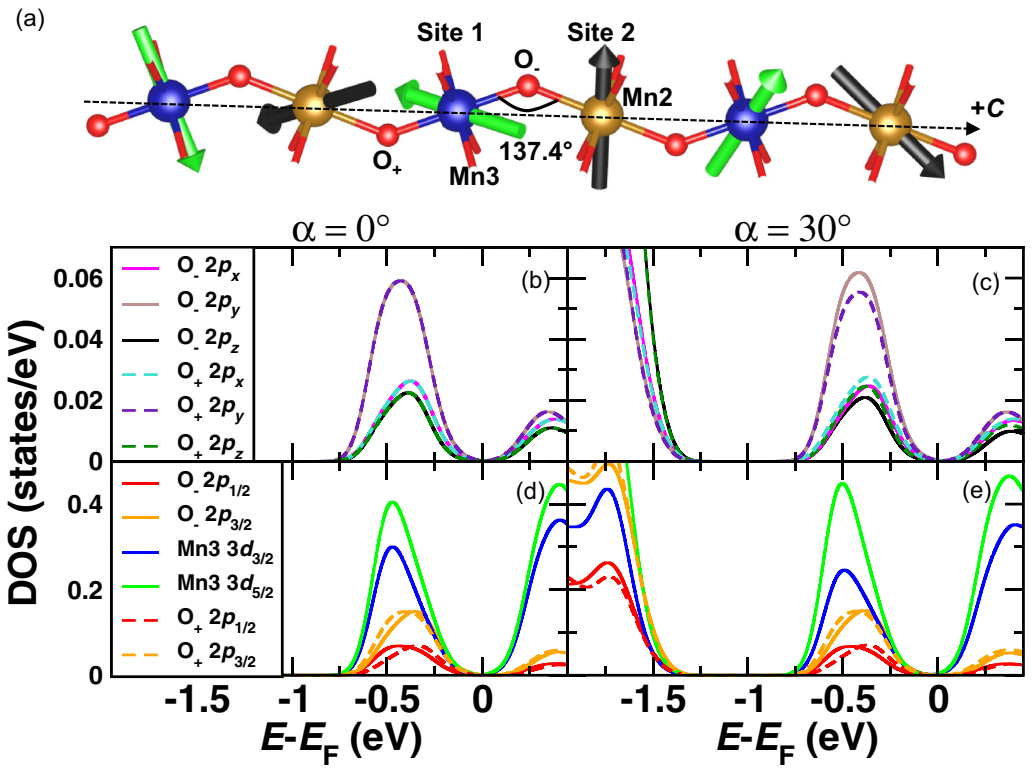

FIG. 3. (a) The Mn2-O-Mn3 chain forms a zig-zag pattern with a bond angle of 137.4°. Orbital-projected density of states for all $2p$-orbital subshells of O_+ (solid lines) and O_- (dashed lines) when (b) $\alpha = 0°$ and (c) $\alpha = 30°$. The spin-orbit coupled states when (d) $\alpha = 0°$ and (e) $\alpha = 30°$. The charge density redistribution along the Mn3-O bonds is evidenced by the changes in the orbital mixing involving O_+ vs O_- when $\alpha = 30°$.

The first term is the nonrelativistic, isotropic Heisenberg symmetric exchange energy ($H_{\rm SE}$), and the second term is the relativistic, anisotropic DM antisymmetric exchange energy ($H_{\rm DM}$), between spin sites 1 and 2. J_{12} is the exchange coupling constant, and the DM vector is defined to be $\boldsymbol{D}_{12} \propto \boldsymbol{r}_1 \times \boldsymbol{r}_2$, where $\boldsymbol{r}_1$ and $\boldsymbol{r}_2$ are vectors connecting each metal to the intersite ligand.

We propose that the exchange coupling constant, J_{12}, can exhibit a dependence on the exchange interaction itself so that the symmetric exchange Hamiltonian has a quadratic term, $(\boldsymbol{S}_1 \cdot \boldsymbol{S}_2)^2$, mediated by Hubbard J that is now distinguished as $J_{\rm Hub}$:

$$H_{\rm SE} = J_{12}(\boldsymbol{S}_1 \cdot \boldsymbol{S}_2)[1 + \gamma J_{\rm Hub}(\boldsymbol{S}_1 \cdot \boldsymbol{S}_2)]. \quad (3)$$

Here, γ is a parameter with a unit of eV^{-1}, such that the quantity $\gamma J_{\rm Hub}$ is dimensionless.

We consider the local hexagonal structure from Fig. 1(d) and the six Mn2-O-Mn3 spin-spin interactions within the B-site helicoidal spiral chains along which the charge redistribution is found to be highly localized. Mn3 spin is designated as $\boldsymbol{S}_{\rm Mn3}$, whereas Mn2 spins of layer I are designated as $\boldsymbol{S}_{\rm I}$ and Mn2 spins of layer V are designated as $\boldsymbol{S}_{\rm V}$. The total exchange energy, with the above dependence on $J_{\rm Hub}$, is given by [76]

$$\begin{aligned} E_{\rm tot} &= E_{\rm Mn3\text{-}V} + E_{\rm Mn3\text{-}I} \\ &= 3J\left[\cos\alpha + \frac{\gamma J_{\rm Hub}}{2}(1 + 2\sin^2\alpha)\right] - 3D^z \sin\alpha. \end{aligned} \quad (4)$$

Because we use the commensurate ionic structure without orbital modulation, $J_{\rm Mn3\text{-}V} = J_{\rm Mn3\text{-}I} = J$ [39,40]. Furthermore, $J < 0$ [37] because charge ordering along the helicoidal spiral chain promotes ferromagnetic exchange, with antiferromagnetic interactions weakened by the large deviation of Mn3-O-Mn2 bond angles from 180° [40]. This reasoning is consistent with our fit of $J = -4.39$ meV based on the aforementioned energy difference of 0.54 meV between $\alpha = 0$ and 30° in the absence of SOC. Our J value is also in agreement with the one reported by Lu *et al.* (−2.96 meV) [37].

The minimum of the total energy in Eq. (6) depends on the relative strength of the exchange interactions and $J_{\rm Hub}$. Setting $\frac{dE_{\rm tot}}{d\alpha} = 0$,

$$-\frac{D^z}{J} = \tan\alpha_{\rm min} - 2\gamma J_{\rm Hub}\sin\alpha_{\rm min}, \quad (5)$$

where $\alpha_{\rm min}$ is the value that minimizes the energy. In the absence of SOC, i.e., $D^z = 0$,

$$\alpha_{\rm min} = \begin{cases} 0^\circ & \text{if} \quad 0 \leqslant \gamma J_{\rm Hub} \leqslant 0.5, \\ \pm\cos^{-1}\frac{1}{2\gamma J_{\rm Hub}} & \text{if} \quad \gamma J_{\rm Hub} > 0.5. \end{cases} \quad (6)$$

In other words, the nonrelativistic total energy in Eq. (4) turns into a local double-well potential, with minima occurring at nonzero α above a certain threshold value of $\gamma J_{\rm Hub} = 0.5$. A fit of $\gamma \approx 0.5\ \mathrm{eV}^{-1}$ can be derived from our results, where $\alpha_{\rm min} \approx 30^\circ$ is achieved with $J_{\rm Hub} \gtrsim 1$ eV [65].

Previous DFT + $U_{\rm eff}$ study (i.e., $J_{\rm Hub} = 0$) by Lu *et al.* [37] reported $|D/J| \approx 0.73$ corresponding to $|\alpha_{\rm min}| = 36.2^\circ$, indicating unusually strong DM interaction compared to other magnetic insulators where $|D/J| \lesssim 0.1$ is usually expected [80]. In addition to Hubbard J, DM interaction is indeed also capable of lowering the total energy by shifting α away from 0° (Table II), which is consistent with our DFT results where SOC induces a small deviation of α away from 0° when $J_{\rm Hub} = 0$ [65].

By allowing Mn3 spins to cant away from the $\alpha = 0^\circ$ configuration, Hubbard J causes Mn3-I interaction (30° alignment) to become more ferromagnetic than Mn3-V interaction (90° alignment). This leads to an unequal enhancement of double exchange, i.e., a weak exchange striction, where the electrons are slightly more localized in the Mn3-V regime than in the Mn3-I regime (Fig. 2). The effect of this exchange striction on the charge density is manifested in the orbital-projected density of states (PDOS) along the O_+–Mn3–O_-–Mn2 chain [Fig. 3(a)]. O_+ and O_- refer to the oxygens along the reduced and enhanced charge density bonds, respectively. The total $2p$ PDOS (not shown) exhibits no difference between $\alpha = 0$ and ≈30°. However, a significant difference arises within the p_x, p_y, and p_z orbitals [Figs. 3(b) and 3(c)]. At $\alpha \approx 30^\circ$, these orbital densities of O_+ and O_- are inequivalent, thereby enhancing the mixing between Mn3 $3d$ and O_- $2p$.

We also examine the densities of the spin-orbit coupled states, indexed as $J = L + S$ [Figs. 3(d) and 3(e)]. The splitting between Mn3 $3d_{\frac{3}{2}}$ and $3d_{\frac{5}{2}}$ is enlarged when $\alpha \approx 30^\circ$, resulting in more mixing between $3d_{\frac{5}{2}}$ and O_- $2p$. These analyses provide an orbitally resolved understanding of how the charge density is redistributed through the Mn3-O bonds.

IV. SUMMARY AND CONCLUSIONS

In summary, our DFT+U+J+SOC calculations demonstrate that $CaMn_7O_{12}$ adopts noncollinear magnetism due to the geometric frustration within the hexagonal Kagome lattice, and the Mn3 spins adopt the noncentrosymmetric (30°, 90°) configuration stabilized relativistically by DM interaction as well as by fully anisotropic Hubbard J. The resulting Berry phase polarization is nearly purely electronic in nature with negligible Mn displacements. The polarization is coupled to the spin helicity, vanishing and reversing its direction at the centrosymmetric (60°, 60°) configuration. The charge density redistribution along the Mn3-O bonds, as evidenced by our orbital-projected density of states, originates nonrelativistically from weak exchange striction within the commensurate structure. Our findings suggest the existence of spin-induced ferroelectricity in the nearly inversion-symmetric ionic lattice, opening the avenue for ultrafast magnetoelectric effect in a single ferroelectric-magnetic domain.

ACKNOWLEDGMENTS

We thank A. Brooks Harris, Eugene J. Mele, and Charles Kane for fruitful discussions. J.S.L. wishes to thank the Vagelos Integrated Program in Energy Research at the University of Pennsylvania. D.S.-G. was supported by the NSF under Grant No. DMR-1719353. A.M.R. was supported by the U.S. Department of Energy, under Grant No. DE-FG02-07ER46431. The authors acknowledge computational support from the High-Performance Computing Modernization Office of the U.S. Department of Defense, as well as the National Energy Research Scientific Computing center.

[1] N. A. Spaldin and M. Fiebig, Science **309**, 391 (2005).
[2] M. Fiebig, J. Phys. D **38**, R123 (2005).
[3] D. Khomskii, Physics **2**, 20 (2009).
[4] Y.-H. Chu, L. W. Martin, M. B. Holcomb, M. Gajek, S.-J. Han, Q. He, N. Balke, C.-H. Yang, D. Lee, W. Hu, Q. Zhan, P.-L. Yang, A. Fraile-Rodriguez, A. Scholl, S. X. Wang, and R. Ramesh, Nat. Mater. **7**, 478 (2008).
[5] D. Lebeugle, A. Mougin, M. Viret, D. Colson, and L. Ranno, Phys. Rev. Lett. **103**, 257601 (2009).
[6] G. Catalan and J. F. Scott, Adv. Mater. **21**, 2463 (2009).
[7] J. van den Brink and D. I. Khomskii, J. Phys.: Condens. Matter **20**, 434217 (2008).
[8] B. B. van Aken, T. T. M. Palstra, A. Filippetti, and N. A. Spaldin, Nat. Mater. **3**, 164 (2004).
[9] N. A. Benedek and C. J. Fennie, Phys. Rev. Lett. **106**, 107204 (2011).
[10] M. Kenzelmann, A. B. Harris, S. Jonas, C. Broholm, J. Schefer, S. B. Kim, C. L. Zhang, S.-W. Cheong, O. P. Vajk, and J. W. Lynn, Phys. Rev. Lett. **95**, 087206 (2005).
[11] T. Kimura, T. Goto, H. Shintani, K. Ishizaka, T. Arima, and Y. Tokura, Nature (London) **426**, 55 (2003).
[12] T. Goto, T. Kimura, G. Lawes, A. P. Ramirez, and Y. Tokura, Phys. Rev. Lett. **92**, 257201 (2004).
[13] H. J. Xiang, S.-H. Wei, M.-H. Whangbo, and J. L. F. D. Silva, Phys. Rev. Lett. **101**, 037209 (2008).
[14] A. Malashevich and D. Vanderbilt, Phys. Rev. Lett. **101**, 037210 (2008).
[15] V. Y. Pomjakushin, M. Kenzelmann, A. Dönni, A. B. Harris, T. Nakajima, S. Mitsuda, M. Tachibana, L. Keller, J. Mesot, H. Kitazawa, and E. Takayama-Muromachi, New J. Phys. **11**, 043019 (2009).
[16] Y. Yamasaki, S. Miyasaka, Y. Kaneko, J.-P. He, T. Arima, and Y. Tokura, Phys. Rev. Lett. **96**, 207204 (2006).
[17] K. Taniguchi, N. Abe, T. Takenobu, Y. Iwasa, and T. Arima, Phys. Rev. Lett. **97**, 097203 (2006).
[18] T.-h. Arima, J. Phys. Soc. Jpn. **76**, 073702 (2007).
[19] M. Kenzelmann, G. Lawes, A. B. Harris, G. Gasparovic, C. Broholm, A. P. Ramirez, G. A. Jorge, M. Jaime, S. Park, Q. Huang, A. Y. Shapiro, and L. A. Demianets, Phys. Rev. Lett. **98**, 267205 (2007).
[20] T. Kimura, J. C. Lashley, and A. P. Ramirez, Phys. Rev. B **73**, 220401 (2006).
[21] S. Seki, Y. Onose, and Y. Tokura, Phys. Rev. Lett. **101**, 067204 (2008).
[22] K. Kimura, H. Nakamura, K. Ohgushi, and T. Kimura, Phys. Rev. B **78**, 140401 (2008).
[23] Y. J. Choi, H. T. Yi, S. Lee, Q. Huang, V. Kiryukhin, and S.-W. Cheong, Phys. Rev. Lett. **100**, 047601 (2008).
[24] I. A. Sergienko, C. Şen, and E. Dagotto, Phys. Rev. Lett. **97**, 227204 (2006).
[25] Y. Tokunaga, S. Iguchi, T. Arima, and Y. Tokura, Phys. Rev. Lett. **101**, 097205 (2008).
[26] G. Lawes, A. B. Harris, T. Kimura, N. Rogado, R. J. Cava, A. Aharony, O. Entin-Wohlman, T. Yildrim, M. Kenzelmann, C. Broholm, and A. P. Ramirez, Phys. Rev. Lett. **95**, 087205 (2005).
[27] K. Wang, J.-M. Liu, and Z. Ren, Adv. Phys. **58**, 321 (2009).
[28] S.-W. Cheong and M. Mostovoy, Nat. Mater. **6**, 13 (2007).
[29] Y. Tokura, S. Seki, and N. Nagaosa, Rep. Prog. Phys. **77**, 076501 (2014).
[30] E. Bousquet and A. Cano, J. Phys.: Condens. Matter **28**, 123001 (2016).
[31] H. Katsura, N. Nagaosa, and A. V. Balatsky, Phys. Rev. Lett. **95**, 057205 (2005).
[32] H. Murakawa, Y. Onose, S. Miyahara, N. Furukawa, and Y. Tokura, Phys. Rev. B **85**, 174106 (2012).
[33] C. Jia, S. Onoda, N. Nagaosa, and J. H. Han, Phys. Rev. B **74**, 224444 (2006).
[34] H. J. Xiang, P. S. Wang, M.-H. Whangbo, and X. G. Gong, Phys. Rev. B **88**, 054404 (2013).
[35] H. J. Xiang, E. J. Kan, Y. Zhang, M.-H. Whangbo, and X. G. Gong, Phys. Rev. Lett. **107**, 157202 (2011).
[36] R. D. Johnson, L. C. Chapon, D. D. Khalyavin, P. Manuel, P. G. Radaelli, and C. Martin, Phys. Rev. Lett. **108**, 067201 (2012).
[37] X. Z. Lu, M.-H. Whangbo, S. Dong, X. G. Gong, and H. J. Xiang, Phys. Rev. Lett. **108**, 187204 (2012).
[38] J. T. Zhang, X. M. Lu, J. Zhou, H. Sun, F. Z. Huang, and J. S. Zhu, Phys. Rev. B **87**, 075127 (2013).
[39] K. Cao, R. D. Johnson, N. Perks, F. Giustino, and P. G. Radaelli, Phys. Rev. B **91**, 064422 (2015).
[40] N. J. Perks, R. D. Johnson, C. Martin, L. C. Chapon, and P. G. Radaelli, Nat. Commun. **3**, 1277 (2012).
[41] T. Locherer, R. Dinnebier, R. Kremer, M. Greenblatt, and M. Jansen, J. Solid State Chem. **190**, 277 (2012).
[42] I. O. Troyanchuk, L. S. Lobanovsky, N. V. Kasper, M. Hervieu, A. Maignan, C. Michel, H. Szymczak, and A. Szewczyk, Phys. Rev. B **58**, 14903 (1998).
[43] A. Huon, A. C. Lang, D. Saldana-Greco, J. S. Lim, E. J. Moon, A. M. Rappe, M. L. Taheri, and S. J. May, Appl. Phys. Lett. **107**, 142901 (2015).
[44] R. D. Johnson, D. D. Khalyavin, P. Manuel, A. Bombardi, C. Martin, L. C. Chapon, and P. G. Radaelli, Phys. Rev. B **93**, 180403(R) (2016).
[45] D. Hobbs and J. Hafner, *Noncollinear Magnetism*, Annals of the Marie Curie Fellowship Association Vol. 4 (2006), pp. 1–6.
[46] K. T. Delaney, M. Mostovoy, and N. A. Spaldin, Phys. Rev. Lett. **102**, 157203 (2009).
[47] K. Matan, B. M. Bartlett, J. S. Helton, V. Sikolenko, S. Mat'aš, K. Prokeš, Y. Chen, J. W. Lynn, D. Grohol, T. J. Sato, M. Tokunaga, D. G. Nocera, and Y. S. Lee, Phys. Rev. B **83**, 214406 (2011).
[48] J.-Q. Dai, H. Zhang, and Y.-M. Song, J. Magn. Magn. Mater. **396**, 135 (2015).
[49] J.-Q. Dai, J. Magn. Magn. Mater. **424**, 314 (2017).
[50] R. Przenioslo, D. Wardecki, W. Slawinski, I. Sosnowska, and L. Keller, Physica B **428**, 27 (2013).
[51] G. Zhang, S. Dong, Z. Yan, Y. Guo, Q. Zhang, S. Yunoki, E. Dagotto, and J.-M. Liu, Phys. Rev. B **84**, 174413 (2011).
[52] J. P. Perdew, A. Ruzsinszky, G. I. Csonka, O. A. Vydrov, G. E. Scuseria, L. A. Constantin, X. Zhou, and K. Burke, Phys. Rev. Lett. **100**, 136406 (2008).
[53] A. I. Liechtenstein, V. I. Anisimov, and J. Zaanen, Phys. Rev. B **52**, R5467 (1995).
[54] B. Himmetoglu, R. M. Wentzcovitch, and M. Cococcioni, Phys. Rev. B **84**, 115108 (2011).
[55] P. Giannozzi, S. Baroni, N. Bonini, M. Calandra, R. Car, C. Cavazzoni, D. Ceresoli, G. L. Chiarotti, M. Cococcioni, I. Dabo, A. D. Corso, S. de Gironcoli, S. Fabris, G. Fratesi, R. Gebauer, U. Gerstmann, C. Gougoussis, A. Kokalj, M. Lazzeri, L. Martin-Samos, N. Marzari, F. Mauri, R. Mazzarello, S. Paolini, A. Pasquarello, L. Paulatto, C. Sbraccia, S. Scandolo,

G. Sclauzero, A. P. Seitsonen, A. Smogunov, P. Umari, and R. M. Wentzcovitch, J. Phys.: Condens. Matter **21**, 395502 (2009).
[56] E. Bousquet and N. Spaldin, Phys. Rev. B **82**, 220402(R) (2010).
[57] A. M. Rappe, K. M. Rabe, E. Kaxiras, and J. D. Joannopoulos, Phys. Rev. B **41**, 1227 (1990).
[58] N. J. Ramer and A. M. Rappe, Phys. Rev. B **59**, 12471 (1999).
[59] http://opium.sourceforge.net.
[60] G. Theurich and N. A. Hill, Phys. Rev. B **64**, 073106 (2001).
[61] S. G. Louie, S. Froyen, and M. L. Cohen, Phys. Rev. B **26**, 1738 (1982).
[62] M. Fuchs and M. Scheffler, Comput. Phys. Commun. **119**, 67 (1999).
[63] D. Porezag, M. R. Pederson, and A. Y. Liu, Phys. Rev. B **60**, 14132 (1999).
[64] H. J. Monkhorst and J. D. Pack, Phys. Rev. B **13**, 5188 (1976).
[65] See Sec. I, Supplemental Material at http://link.aps.org/supplemental/10.1103/PhysRevB.97.045115 for details on Hubbard U and J values.
[66] W. Slawinski, R. Przenioslo, I. Sosnowska, D. Wardecki, A. N. Fitch, M. Bieringer, and J. B. Jasinski, J. Solid State Chem. **198**, 392 (2013).
[67] R. D. King-Smith and D. Vanderbilt, Phys. Rev. B **47**, 1651 (1993).
[68] See Sec. II, Supplemental Material at http://link.aps.org/supplemental/10.1103/PhysRevB.97.045115 for details on Berry phase polarization.
[69] See Sec. III, Supplemental Material at http://link.aps.org/supplemental/10.1103/PhysRevB.97.045115 for details on Mn3 ionic displacements.
[70] See Sec. IV, Supplemental Material at http://link.aps.org/supplemental/10.1103/PhysRevB.97.045115 for details on inversion symmetry breaking by the Mn3-Mn2 helicoidal spin spiral.
[71] S. Picozzi, K. Yamauchi, B. Sanyal, I. A. Sergienko, and E. Dagotto, Phys. Rev. Lett. **99**, 227201 (2007).
[72] I. V. Solovyev and Z. V. Pchelkina, New J. Phys. **10**, 073021 (2008).
[73] P. Barone, K. Yamauchi, and S. Picozzi, Phys. Rev. Lett. **106**, 077201 (2011).
[74] I. V. Solovyev, Phys. Rev. B **87**, 144403 (2013).
[75] S. L. Dudarev, G. A. Botton, S. Y. Savrasov, C. J. Humphreys, and A. P. Sutton, Phys. Rev. B **57**, 1505 (1998).
[76] See Sec. V, Supplemental Material at http://link.aps.org/supplemental/10.1103/PhysRevB.97.045115 for details on Mn3-Mn2 exchange interactions.
[77] D. A. Tompsett, D. S. Middlemiss, and M. S. Islam, Phys. Rev. B **86**, 205126 (2012).
[78] T. A. Mellan, F. Cora, R. Grau-Crespo, and S. Ismail-Beigi, Phys. Rev. B **92**, 085151 (2015).
[79] J. S. Lim, D. Saldana-Greco, and A. M. Rappe, Phys. Rev. B **94**, 165151 (2016).
[80] T. Moriya, Phys. Rev. **120**, 91 (1960).